

Configurational Temperature of Charge-Stabilized Colloidal Monolayers

Yilong Han and David G. Grier

*Dept. of Physics, James Franck Institute and Institute for Biophysical Dynamics
The University of Chicago, Chicago, IL 60637*

(Dated: November 17, 2018)

Recent theoretical advances show that the temperature of a system in equilibrium can be measured from static snapshots of its constituents' instantaneous configurations, without regard to their dynamics. We report the first measurements of the configurational temperature in an experimental system. In particular, we introduce a hierarchy of hyperconfigurational temperature definitions, which we use to analyze monolayers of charge-stabilized colloidal spheres. Equality of the hyperconfigurational and bulk thermodynamic temperatures provides previously lacking thermodynamic self-consistency checks for the measured colloidal pair potentials, and thereby casts new light on anomalous like-charge colloidal attractions induced by geometric confinement.

The temperature of an equilibrium ensemble of particles is defined conventionally in terms of the particles' mean kinetic energy, without regard for their instantaneous positions. In 1997, Rugh pointed out that the temperature can also emerge from other ensemble averages over geometrical and dynamical quantities [1]. This notion is expressed more generally [2, 3] as

$$k_B T = \frac{\langle \nabla \mathcal{H} \cdot \mathbf{B}(\mathbf{\Gamma}) \rangle}{\langle \nabla \cdot \mathbf{B}(\mathbf{\Gamma}) \rangle}, \quad (1)$$

where angle brackets indicate an ensemble (or time) average, $\mathbf{\Gamma} = \{q_1, \dots, q_{3N}, p_1, \dots, p_{3N}\}$ is the instantaneous set of $3N$ generalized coordinates q_j and their conjugate momenta p_j for an N -particle system, $\mathcal{H} = \sum_{j=1}^{3N} p_j^2/(2m) + V(\{q_j\})$ is the Hamiltonian associated with the conservative N -particle potential $V(\{q_j\})$, and $\mathbf{B}(\mathbf{\Gamma})$ is an *arbitrary* vector field selected so that both the numerator and denominator of Eq. (1) are finite and the numerator grows more slowly than e^N in the thermodynamic limit. Choosing $\mathbf{B}(\mathbf{\Gamma}) = \{0, \dots, 0, p_1, \dots, p_{3N}\}$ yields the usual kinetic definition of temperature. Choosing instead $\mathbf{B}(\mathbf{\Gamma}) = -\nabla V(\{q_i\})$ yields a formally equivalent result,

$$k_B T_{\text{config}} = \frac{\langle |\nabla V|^2 \rangle}{\langle \nabla^2 V \rangle}, \quad (2)$$

which depends only on the particles' instantaneous configuration, and not on their momenta. Variants of Eq. (2) have been widely adopted in molecular dynamics simulations [4, 5], but have not previously been applied to experiments.

In this Letter, we use the configurational temperature formalism to probe macroionic interactions in monolayers of charged colloidal spheres dispersed in water and confined between parallel glass plates. These measurements provide sensitive self-consistency tests for the measured inter-particle pair potentials, and thereby provide new insights into the long-standing conundrum of anomalous attractions in geometrically confined charge-stabilized dispersions.

Directly applying Eq. (2) requires the full N -particle free energy, which is rarely available. Simplified forms emerge for systems satisfying certain conditions. For example, if $V(\{q_i\})$ is the linear superposition of pair potentials, $u(r)$, then Eq. (2) reduces to [4],

$$k_B T_{\text{conf}} = - \frac{\langle \sum_{i=1}^N F_i^2 \rangle}{\langle \sum_{i=1}^N \nabla_i \cdot \mathbf{F}_i \rangle}, \quad (3)$$

where $\mathbf{F}_i = -\sum_{j \neq i} \nabla_i u(r_{ij})$ is the total force on particle i due to its interactions with other particles, ∇_i is the gradient with respect to the i -th particle's position, \mathbf{r}_i , and $r_{ij} = |\mathbf{r}_i - \mathbf{r}_j|$ is the center-to-center separation between particles i and j . The temperature is reflected in the instantaneous distribution of forces because objects explore more of their potential energy landscape as the temperature increases.

Equation (3) may be generalized into a hierarchy of *hyperconfigurational* temperatures by choosing $\mathbf{B}(\mathbf{\Gamma}) = \{F_i^s\}$:

$$k_B T_h^{(s)} = - \frac{\langle \sum_{i=1}^N F_i^{s+1} \rangle}{\langle s \sum_{i=1}^N F_i^{s-1} \nabla_i \cdot \mathbf{F}_i \rangle}, \quad (4)$$

for $s > 0$. These higher moments are more sensitive to the input potential's detailed structure than $T_{\text{conf}} = T_h^{(1)}$. They also can be applied to three-dimensional systems with long-ranged $1/r$ potentials, for which T_{conf} is ill-defined.

The same hierarchy also may be derived from the classical hypervirial theorem [7], $\langle \{f, \mathcal{H}\} \rangle = 0$, where $\{\dots\}$ is the Poisson bracket, by selecting $f(\mathbf{\Gamma}) = \sum_{j=1}^N p_j F_j^s$. More generally, $f(\mathbf{\Gamma})$ can be any finite-valued function that does not explicitly depend on time.

For systems with short-ranged potentials, dropping additional terms of $\mathcal{O}(1/N)$ from Eq. (1) yields [2]:

$$k_B T_{\text{con1}} = - \left\langle \frac{\sum_{i=1}^N F_i^2}{\sum_{i=1}^N \nabla_i \cdot \mathbf{F}_i} \right\rangle, \quad \text{and} \quad (5)$$

$$k_B T_{\text{con2}} = - \left\langle \frac{\sum_{i=1}^N \nabla_i \cdot \mathbf{F}_i}{\sum_{i=1}^N F_i^2} \right\rangle^{-1}, \quad (6)$$

the second of which is proposed here for the first time. These definitions' different dependences on sample size N are useful for comparison with $T_h^{(s)}$.

Temperature definitions based on configurational information are ideal for studying colloidal spheres dispersed in viscous fluids such as water. The fluid acts as a heat bath at temperature T . It also randomizes the particles' motions over intervals longer than the viscous relaxation time, typically measured in microseconds. As a result, the colloids' instantaneous momenta are not easily accessible. Their positions, however, are readily measured using standard methods of digital video microscopy [6]. Calculating the temperature from the resulting positional data then requires accurate knowledge of the colloids' interactions.

The mean-field theory for macroionic interactions [8] predicts that charge-stabilized colloidal spheres should repel each other through a screened-Coulomb potential:

$$\beta u(r) = Z^2 \lambda_B \frac{\exp(\kappa\sigma)}{(1 + \frac{\kappa\sigma}{2})^2} \frac{\exp(-\kappa r)}{r}, \quad (7)$$

where $\beta^{-1} = k_B T$ is the heat bath's thermal energy scale, σ is the spheres' diameter, r is their center-to-center separation, Z is the effective charge number on each sphere and $\lambda_B = e^2 / (4\pi\epsilon k_B T)$ is the Bjerrum length in a medium of dielectric constant ϵ . The Debye-Hückel screening length κ^{-1} sets the range of the effective electrostatic interaction and depends on the concentration c of (monovalent) ions through $\kappa^2 = 4\pi c \lambda_B$.

Despite its success at explaining bulk colloidal phenomena [8], mean-field theory qualitatively fails [9] to explain the strong and long-ranged attractions observed when charged spheres are confined between parallel glass walls [6, 10, 11, 12]. The crossover from monotonic repulsion to long-ranged attraction with increasing confinement is demonstrated in Fig. 1. Efforts to explain this anomaly through non-mean-field mechanisms so far have not yielded the experimentally observed effect [13]. Given the apparent difficulty of explaining anomalous attractions on the basis of colloidal electrostatics or electrodynamics, various other explanations have been proposed, most of which focus on possible experimental artifacts. For example, nonequilibrium hydrodynamic coupling has been shown [14] to explain one measurement based on optical tweezer manipulation [15], but cannot be relevant for measurements based on video microscopy of colloid in equilibrium [10, 11, 12, 16, 17]. Concern also has been raised that such imaging measurements can fall victim to correlated artifacts due to statistical fluctuations [17]. We have shown, however, that anomalous attractions still are clearly resolved given adequate statistics [12]. A still greater concern is that uncorrected many-body artifacts could mimic attractions in purely repulsive dispersions. Such artifacts certainly can arise at high densities, as has been demonstrated experimentally [18]. Evidence

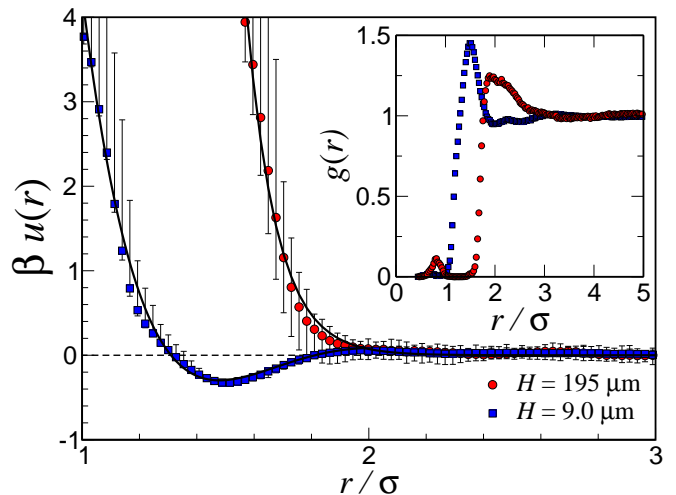


FIG. 1: Pair potentials $u(r)$ for silica colloid $\sigma = 1.58 \mu\text{m}$ in diameter extracted from the measured radial distribution functions $g(r)$ using the HNC approximation for suspensions at $H = 9 \mu\text{m}$, $n\sigma^2 = 0.0654$ (squares) and $H = 195 \mu\text{m}$, $n\sigma^2 = 0.0797$ (circles). Solid curves are, respectively, fits to a 5-th order polynomial and to Eq. (7) ($\kappa^{-1} = 180 \pm 10 \text{ nm}$, $Z = 6500 \pm 1000$).

for pairwise additivity at lower densities has relied principally on comparisons over a range of concentrations, for which variations in chemical environment could mask other effects.

We resolve all such ambiguities by exploiting the configurational temperatures' sensitivity to inaccuracies in the input potential as self-consistency tests for colloidal interaction measurements. In particular, we use pair potentials measured according to Refs. [6], [12] and [17] to compute the configurational temperature of geometrically confined colloidal monolayers and compare the results with the bulk thermodynamic temperature, with $T_h^{(s)} = T$ signaling thermodynamic self-consistency. Deviations could result from a breakdown of pairwise additivity in a system with non-trivial many-body interactions, a departure from equilibrium in a system subjected to hydrodynamic forces, or simply inaccuracy in $u(r)$.

Our samples consist of uniform silica spheres $\sigma = 1.58 \pm 0.03 \mu\text{m}$ in diameter (Duke Scientific Lot 24169) dispersed in deionized water and loaded into hermetically sealed sample volumes formed by bonding the edges of glass #1.5 coverslips to the surfaces of glass microscope slides. The separation H between these surfaces is set during construction and establishes the degree of confinement. Reservoirs of mixed bed ion exchange resin maintain the ionic strength below $c \approx 10 \mu\text{M}$, corresponding to a Debye-Hückel screening length $\kappa^{-1} \gtrsim 150 \text{ nm}$. Under these conditions, both the silica spheres and the glass walls develop negative surface charge densities of roughly $10^3 e_0 \mu\text{m}^{-2}$, where e_0 is the electron charge [19]. Samples are mounted on the stage of a Zeiss Ax-

iovert 100 STV microscope, after which the dense silica spheres rapidly sediment into a monolayer roughly $h = 900$ nm above the coverslip with out-of-plane fluctuations smaller than 300 nm. The bright-field imaging system provides a magnification of 212 nm/pixel on a Hitachi TI-11A monochrome CCD camera. The resulting video stream is recorded and digitized into 60 deinterlaced video fields per second, each of which is analyzed to yield the instantaneous distribution

$$\rho(\mathbf{r}) = \sum_{i=1}^{N(t)} \delta(\mathbf{r} - \mathbf{r}_i(t)) \quad (8)$$

of $N(t)$ spheres at locations $\mathbf{r}_i(t)$ at time t . Measurements were performed at room temperature over periods of roughly one hour, with temperature fluctuations smaller than ± 1 K over the course of any measurement.

From $\rho(\mathbf{r}, t)$, we calculate the radial distribution function,

$$g(r) = \frac{1}{n^2} \langle \rho(\mathbf{r}' - \mathbf{r}, t) \rho(\mathbf{r}', t) \rangle, \quad (9)$$

where $n = N/A$ is the areal density of $N = \langle N(t) \rangle$ particles in the field of view of area A , and the angle brackets indicate averages over angles and time. Assuming that the system is in equilibrium and that its interactions are isotropic and pairwise additive, $g(r)$ may be inverted to obtain an estimate for $u(r)$ [10, 11]. At low enough densities, the Boltzmann distribution provides the necessary relationship: $\beta u(r) = -\lim_{n \rightarrow 0} \ln g(r)$. Unfortunately, the need to sample $g(r)$ adequately in a limited field of view requires higher concentrations [12, 17], with $0.05 < n\sigma^2 < 0.1$ being typical for our experiments. We extract candidate pair potentials $u(r)$ such as the examples in Fig. 1 using the liquid-structure inversion method based on the Ornstein-Zernike equation with hypernetted-chain (HNC) and Percus-Yevick (PY) closures [11, 12, 17]. As we have reported previously, the sedimented silica spheres repel each other as predicted by Eq. (7) at the largest inter-plated separations considered, $H = 200 \mu\text{m}$ [12, 17]. Reducing H does not perceptibly change the spheres' equilibrium height h above the lower glass wall, yet nonetheless introduces a minimum into $u(r)$ consistent with a long-ranged attraction [12]. The example in Fig. 1 at $H = 9 \mu\text{m}$ has a minimum roughly $0.3 k_B T$ deep at $r = 1.5\sigma$. Well-resolved minima are evident for spacings as large as $H \leq 30 \mu\text{m}$.

Even the small amount of scatter in the measured pair potentials yields unacceptably large fluctuations in the derivatives used to calculate the configurational temperatures. We avoid this by fitting the experimental data to fifth-order polynomials, as shown in Fig. 1, and using the fits as inputs to Eqs. (4), (5) and (6).

In calculating the total force \mathbf{F}_i on the i -th particle, we must consider all relevant pair interactions. Particles close to the edge of the field of view may have strongly

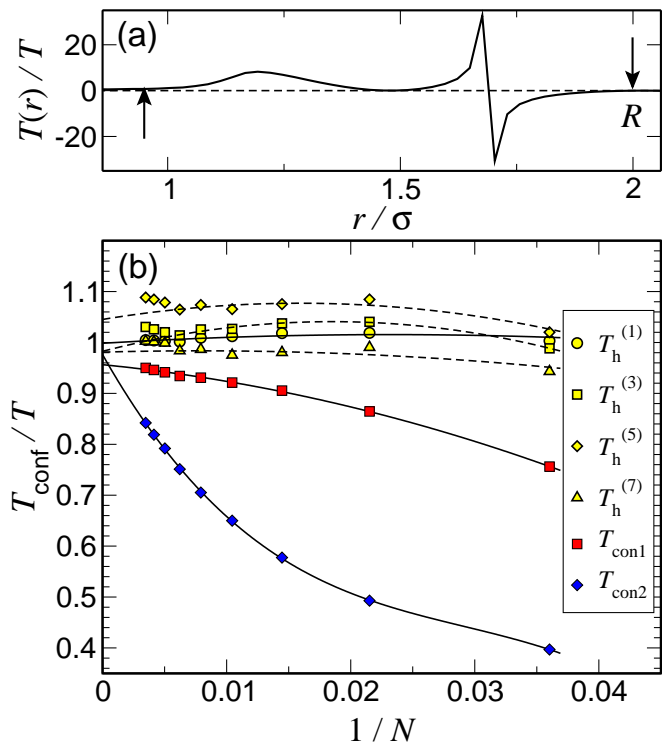


FIG. 2: (a) Estimating the interaction range for the $H = 9 \mu\text{m}$ data set using $T(r)$. Configurational temperatures were calculated over $0.93 < r/\sigma < 2$. (b) Configurational and hyperconfigurational temperatures as a function of sample size, showing finite-size scaling through fits to second-order polynomials in $1/N$ (third-order for T_{con2}).

interacting neighbors just out of view. To avoid errors due to the resulting spuriously unbalanced forces, we restrict ensemble averages to particles farther from the edges than the range R of the interaction. We estimate R by plotting $T(r)/T = 2\pi(r/\sigma) g(r) |\nabla u(r)|^2 / \nabla^2 u(r)$, as shown in Fig. 2(a), which qualitatively gauges contributions to the configurational temperature due to particles at separation r . This is most useful for systems with weak three-body correlations. Typically, $R \lesssim 2.0\sigma$ for our samples.

Sample imperfections such as a small number of dimers also distort the apparent force distribution. We omit such particles from the ensemble averages. By contrast, we include the small number of pair interactions with $r/\sigma \lesssim 1$, which arise from the samples' polydispersity and also because of projection errors due to out-of-plane motions for particles near contact. Omitting these has little effect on T_{conf} , but leads to large systematic errors in higher-order $T_h^{(s)}$.

The restricted sample includes only $N = \mathcal{O}(100)$ particles, hardly the thermodynamic limit. To correct for finite-size effects, we deliberately sub-sample our data, and plot the configurational temperature as a function of $1/N$, as shown in Fig. 2(b). Polynomial fits account for

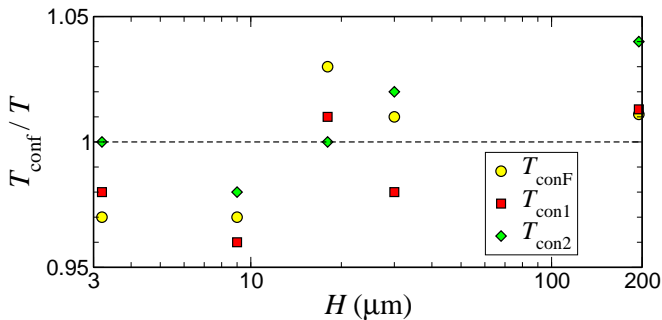


FIG. 3: Configurational temperatures at different plate separations. The uncertainty of each extrapolated temperature is less than 0.02.

the finite-size scaling of Eq. (1), and permit extrapolations to large N . As expected, T_{con1} and T_{con2} are more sensitive to sample size than $T_h^{(s)}$ because their derivations involve ignoring more terms of $\mathcal{O}(1/N)$. Despite these differences, all orders of $T_h^{(s)}$, as well as T_{con1} and T_{con2} , extrapolate to the thermodynamic temperature in the large- N limit. This successful outcome strongly suggests that the experimentally determined potential, including its long-ranged attraction, accurately describes the dispersion's equilibrium pair interactions.

The configurational temperatures are exceedingly sensitive to small variations in $\beta u(r)$, with systematic adjustments as small as 0.01 in the short-range repulsive core leading to variations in the configurational temperature as large as ten percent. Truncating the attractive part of $u(r)$ increases the configurational temperatures by fifty percent. Similarly, failure to precisely correct the imaging system's aspect ratio can lead to large deviations. This potential source of error can be monitored by factoring T_{conF} into components along and transverse to the video scan lines and comparing the results. Deliberately rescaling one axis by 0.01 causes the apparent temperatures along the two directions to differ systematically by as much as ten percent for all samples.

Figure 3 demonstrates that the configurational temperatures are consistent with the thermodynamic temperature over the entire range of wall separations from $H = 3.2 \mu\text{m}$ to $H = 195 \mu\text{m}$, despite variations in the form of the associated pair potential [12]. This allows us to draw several conclusions regarding the nature of confinement-mediated colloidal interactions. Primarily, we conclude that the measured pair potentials accurately and self-consistently describe the colloidal particles' interactions. To the extent that the configurational temperatures are sensitive to local departures from equilibrium [20], the result $T_{\text{conf}}/T = 1.00 \pm 0.04$ for all of our samples suggests that anomalous confinement-induced like-charge colloidal attractions cannot be ascribed to nonequilibrium mechanisms such as hydrodynamic coupling due to transient flows in the sample [21].

In summary, we have calculated the configurational temperature for experimentally determined distributions of colloidal silica spheres using their measured pair potentials as inputs. The success of this procedure provides a thermodynamic self-consistency test for the measured potentials, and thus establishes that confinement induces equilibrium pair attractions between charged colloidal spheres. It furthermore demonstrates the configurational temperature to be a powerful new tool for experimental condensed matter physics.

We are grateful to Owen Jepps for introducing us to the notion of configurational temperatures, to Sven Behrens for extensive discussions, and to the donors of the Petroleum Research Fund of the American Chemical Society for support.

-
- [1] H. H. Rugh, Phys. Rev. Lett. **78**, 772 (1997).
 - [2] O. G. Jepps, G. Ayton, and D. J. Evans, Phys. Rev. E **62**, 4757 (2000).
 - [3] A similar result is obtained in G. Rickayzen and J. G. Powles, J. Chem. Phys. **114**, 4333 (2001).
 - [4] B. D. Butler, G. Ayton, O. G. Jepps, and D. J. Evans, J. Chem. Phys. **109**, 6519 (1998).
 - [5] J. Delhommelle and D. J. Evans, J. Chem. Phys. **117**, 6016 (2002).
 - [6] J. C. Crocker and D. G. Grier, J. Colloid Interface Sci. **179**, 298 (1996).
 - [7] J. O. Hirschfelder, J. Chem. Phys. **33**, 1462 (1960).
 - [8] W. B. Russel, D. A. Saville, and W. R. Schowalter, *Colloidal Dispersions*, (Cambridge University Press, Cambridge, 1989).
 - [9] J. C. Neu, Phys. Rev. Lett. **82**, 1072 (1999); J. E. Sader and D. Y. C. Chan, J. Colloid Interface Sci. **213**, 268 (1999); J. E. Sader and D. Y. C. Chan, Langmuir **16**, 324 (2000); E. Trizac and J.-L. Raimbault, Phys. Rev. E **60**, 6530 (1999).
 - [10] G. M. Kepler and S. Fraden, Phys. Rev. Lett. **73**, 356 (1994).
 - [11] M. D. Carbajal-Tinoco, F. Castro-Román, and J. L. Arauz-Lara, Phys. Rev. E **53**, 3745 (1996).
 - [12] Y. Han and D. G. Grier, Phys. Rev. Lett. **91**, 038302 (2003).
 - [13] A. Gopinathan *et al.*, Europhys. Lett. **57**, 451 (2002).
 - [14] T. Squires and M. P. Brenner, Phys. Rev. Lett. **85**, 4976 (2000).
 - [15] A. E. Larsen and D. G. Grier, Nature **385**, 230 (1997).
 - [16] K. Vondermassen, J. Bongers, A. Mueller, and H. Versmold, Langmuir **10**, 1351 (1994).
 - [17] S. H. Behrens and D. G. Grier, Phys. Rev. E **64**, 050401 (2001).
 - [18] M. Brunner *et al.*, Europhys. Lett. **58**, 926 (2002).
 - [19] S. H. Behrens and D. G. Grier, J. Chem. Phys. **115**, 6716 (2001).
 - [20] J. Ennis and D. J. Evans, Molecular Simulation **26**, 147 (2001).
 - [21] Y. O. Popov, J. Colloid Interface Sci. **252**, 320 (2002).